CrossMark

Effect of Ag doping on structural, optical and photocatalytic activity of tungsten oxide (WO₃) nanoparticles

S. Mohammed Harshulkhan[1] · K. Janaki[2] · G. Velraj[3] · R. Sakthi Ganapthy[1] ·
M. Nagarajan[1]

Abstract In this paper, we discuss the synthesis and characterization of pure and silver (Ag) doped tungsten oxide nanoparticles prepared by microwave irradiation method. The size and morphology were studied by powder X-ray diffraction and the results reveal that the pure and Ag (3 and 10 wt%) doped WO₃ crystallizes in monoclinic structure. TEM analysis shows both pristine and silver doped WO₃ nanoparticles were spherical morphology with a average size from 30 to 40 nm. Scanning electron microscopy result indicates spherical shaped morphology with an average diameter of 40–30 nm, which is in proper agreement with the average crystallite sizes calculated by Scherrer's formula. A considerable red shift in the absorbing band edge and decrease the band gap energy from 3.00 to 2.85 eV for Ag doped samples were observed by using UV-DRS spectra analysis. The defects in crystal and oxygen deficiencies were analyzed by photoluminescence studies. The photocatalytic activities of the pure and Ag doped WO₃ samples were evaluated by the degradation of methylene blue in an aqueous solution under visible light irradiation. The photocatalytic activity for Ag doped WO₃ was much higher than pure WO₃.

✉ S. Mohammed Harshulkhan
harshulkhan21@gmail.com

1 Vinayaka Mission's Kirupananda Variyar Engineering College, Salem, TN 636308, India

2 Government Arts College for Women, Salem, TN 636008, India

3 Department of Physics, Anna University, Chennai, TN 600025, India

1 Introduction

In recent years, photocatalysis technology has received universal attention due to its applications in organic synthesis and the abatement of pollutants in water and air. There has been considerable interest in the synthesis of transition metal oxide semiconductors with diverse morphological structure and the investigation of their properties due to their potential application in electronic, optical, super conductor devices, etc. [1]. It is used to remove the organic pollutant which includes detergent, dyes, pesticides and herbicides under UV-light irradiation. The heterogeneous photocatalyst attracted a considerable attention due to elimination of organic pollutants in water [2–5] and Semiconductor photocatalysts drew attention due to low cost and environmental friendliness. Among the various types of semiconductor photocatalysts (ZnO, TiO₂, SnO₂, In₂O₃) tungsten oxide (WO₃) is highly interesting and have been intensively studied for a long time due to their promising physical and chemical properties [6]. WO₃, an n-type semiconductor with an excellent electrochromic, photochromic and gasochromic properties has been extensively used in variety of applications, including gas and temperature sensing, catalysis, electrochromic windows and displays, flat panel displays, solar energy devices and so on [7]. Tungsten oxide is prepared by various methods like sol–gel method, Chemical precipitation method, hydrothermal process, Sputtering technique and Microwave irradiation method. Among these methods Microwave irradiation method is very simple due its operation, less consumption of time, and purity of the material when compared to other methods [8].

There are several additives and dopants which can improve the photocatalytic performance of WO₃. Chemical doping of WO₃ with metallic (Cu [9], Sn [10], Pd [11] Mn [12] etc.) elements to modify the electronic structures of

semiconductors as well as their surface properties, thus extending their visible light absorbance. In the recent study, it has been reported that the tungsten oxide synthesis was found along with the hydrate group ($WO_3 \cdot H_2O$) by microwave irradiation method [13]. In the present research the pure and silver doped Tungsten oxide without hydrate group were synthesized by Microwave irradiation method. Generally, microwave heating is a promising technology whose applications have been fast growing due to its exclusive effects such as rapid volumetric heating, increased reaction rates and shortened reaction time, improved reaction selectivity and energy saving. Microwave irradiation is effectively used to modify the desired morphology, particle size and high surface areas, this property have huge effects on the photocatalytic properties of semiconductor metal oxides. This paper is reported about structural, optical and photocatalytic activity of pure and Ag doped WO_3 nanoparticles by microwave irradiation method.

2 Experimental procedure

2.1 Material preparation

The precursor solution is prepared by adding tungstic acid in 10 ml of sodium hydroxide (NaOH) solution which results in an yellow colour solution due to proton exchange protocol process. Again Hydrochloric acid (HCl) is added drop by drop till it attains pH value 1. Hydrochloric acid acts as a precipitating agent and also as the medium for the required product to have desired morphology [14]. After accomplishing the pH value, 5 ml of distilled water is added for immediate response of microwave with precursor solution. Eventually the solution was placed into the Microwave oven (2.45 GHz) under optimum power of 360 W for 5 min in air atmosphere. After the irradiation process, the resulted substance was dried in convection mode at 100 °C for 5 min. The silver doped WO_3 was synthesized by adding tungstic acid and silver nitrate at molar ratio (0.03 and 0. 10) in 10 ml of NaOH solution. The above procedure was repeated to obtain the final product. The final product was pale green in colour for pure WO_3 and Ag doped WO_3.

2.2 Characterization techniques

The surface morphology, structural and chemical state of the obtained Nanomaterial was characterized by using X-ray diffraction method (X-ray Diffractometer-XPERT PRO) and FTIR (Spectrum RX I-Perkin Elmer). Transmission Electron Microscope and Selected-area electron diffraction were recorded with JEM2100. High resolution electron microscope were recorded with a accelerating voltage of 200 kV. Optical measurements were carried out in UV–Vis

Spectroscopy (SHIMADZU 3600 UV–Vis Spectrometer), Surface morphology was studied by scanning electron microscopy (SEM) (FEIQUATA250), Elemental analysis were performed by EDAX (FEIQUATA250) and PL spectra were recorded by LS 45 Fluorescence spectrometer.

3 Results and discussion

3.1 XRD analysis

The phase formation and purity of pure and Ag doped WO_3 nanoparticles were investigated by XRD. The microstructure of prepared samples were analysed by X-ray diffraction (XPERT PRO) using Cu Kα wavelength of 1.5405 Å. From the X-ray analysis, it was noted that the diffraction peaks of the pristine WO_3 at 22.99°, 23.46° and 24.24° and for Ag doped WO_3 exhibits the diffraction peak at $2\theta = 23.02°$, 23.49° and 24.27° could correspond to (002), (020) and (200) planes of WO_3 with monoclinic structure [15] as shown in the Fig. 1 and the results are fetch with the standard JCPDS data (card no: 83-0950). Both pure and Ag doped WO_3 can be well indexed to the standard pattern of monoclinic WO_3 with the lattice constants a = 7.300, b = 7.538, c = 7.689 and β = 90.892. In XRD pattern, it confirms that the purity of synthesized materials with the absences of additional peaks. Moreover, the intensity of the peak decreases with the increase in the Ag concentrations. These results clearly indicate that Ag substituted in WO_3 host lattice site.

By using the Debye–Scherrer's equation [16, 17], the average grain size are calculated based on the peaks found in the XRD pattern from $2\theta = 23°$ to 25°. The crystalline size (D) of the pure and Ag doped WO_3 were calculated by using Debye–Scherrer's relation,
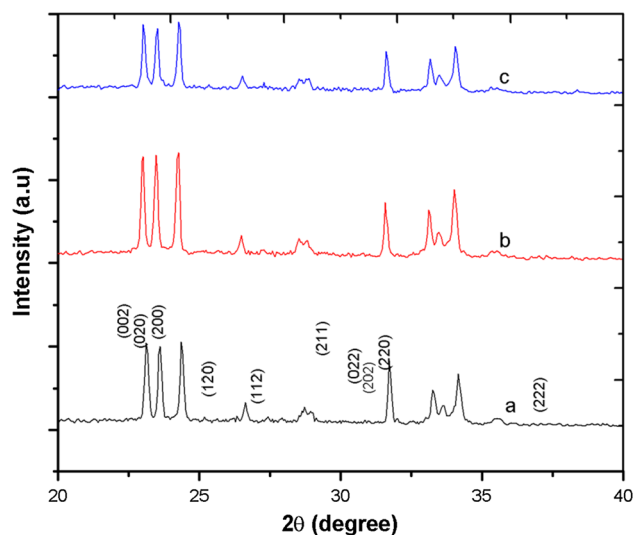
Fig. 1 XRD pattern for (*a*) pure WO_3, (*b*) 3 wt% Ag, (*c*) 10 wt% Ag
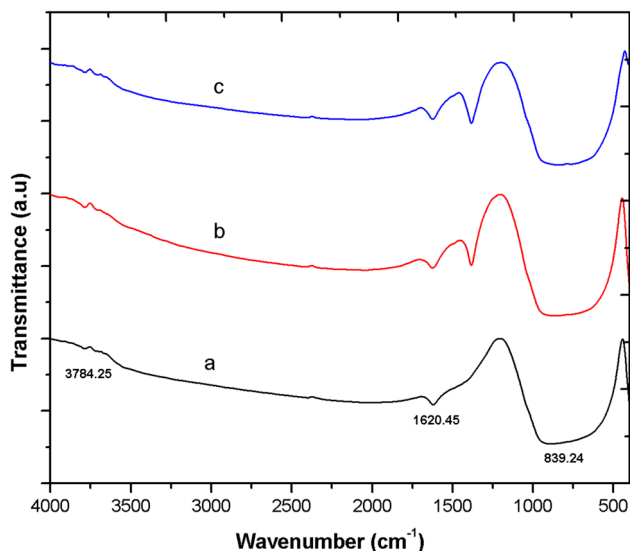
Fig. 2 FTIR spectrum of (*a*) pure WO$_3$, (*b*) 3 wt% Ag, (*c*) 10 wt% Ag

$$D = \frac{0.9\lambda}{\beta \cos\theta} \text{ nm}$$

where β is the full width at half maximum, λ is the X-ray wavelength (0.15406 nm), and θ is the diffraction angle. The average crystallite size is calculated for pure WO$_3$ is 35 and 33, 31 nm for 3 and 10 % of Ag doped WO$_3$. The average crystallite size of pristine WO$_3$ was found to be 35 nm and it was further decreased to 31 nm for 10 wt% Ag doped WO$_3$. The XRD results reveal that the crystalline size has decreased with increase in Ag concentration.

3.2 FTIR analysis

FTIR spectroscopy is a powerful technique to study the crystalline quality structure disorder and defects in doped semiconductor alloy. It gives significant information about local structure change due to incorporation of Ag ions into WO$_3$ host lattice [18]. Figure 2 shows the FTIR spectra of pure and Ag (3 and 10 wt%) doped WO$_3$ in room temperature. The observed wave number, relative intensities obtained from the recorded spectra and the assignments were illustrated in Table 1. The tungsten oxide vibrations are found in the infrared region of 1453–600 cm^{-1} which correspond to W–O stretching, bending and lattice mode [19]. The wave number greater than 3700 cm^{-1} show a very high transmittance due to a low absorption character.

The peak around 1620 cm^{-1} may be assigned to W–OH vibration. The spectrum shows a strong band at 830 cm^{-1} for W–O–W bridging mode [20]. After Ag doping these peaks were shifted to lower wavenumber and this may have been due to the decrease in size of the doped samples.

3.3 UV–visible diffusion reflectance spectroscopy

The optical property of substitution of silver into WO$_3$ site, the sample were characterized by UV–Vis transmission spectra analysis. Figure 3a–c shows the diffusion reflectance spectra of pure and Ag doped WO$_3$ respectively. It was observed that the optical transparency of the pure WO$_3$ decreases with increase in the Ag content. The decrease in the transparency of Ag doped WO$_3$ was attributed to the increase in reflectance due to the presence of the metal ion. A considerable red shift was observed in the absorption edges with the increase of Ag content from 0 to 10 wt%, which indicates the decrease in bandgap of WO$_3$ on doping. The band gap energies (E$_g$) have been calculated using Kubelka–Munk (K–M) model as described below. The K–M model [20] at any wavelength is given by

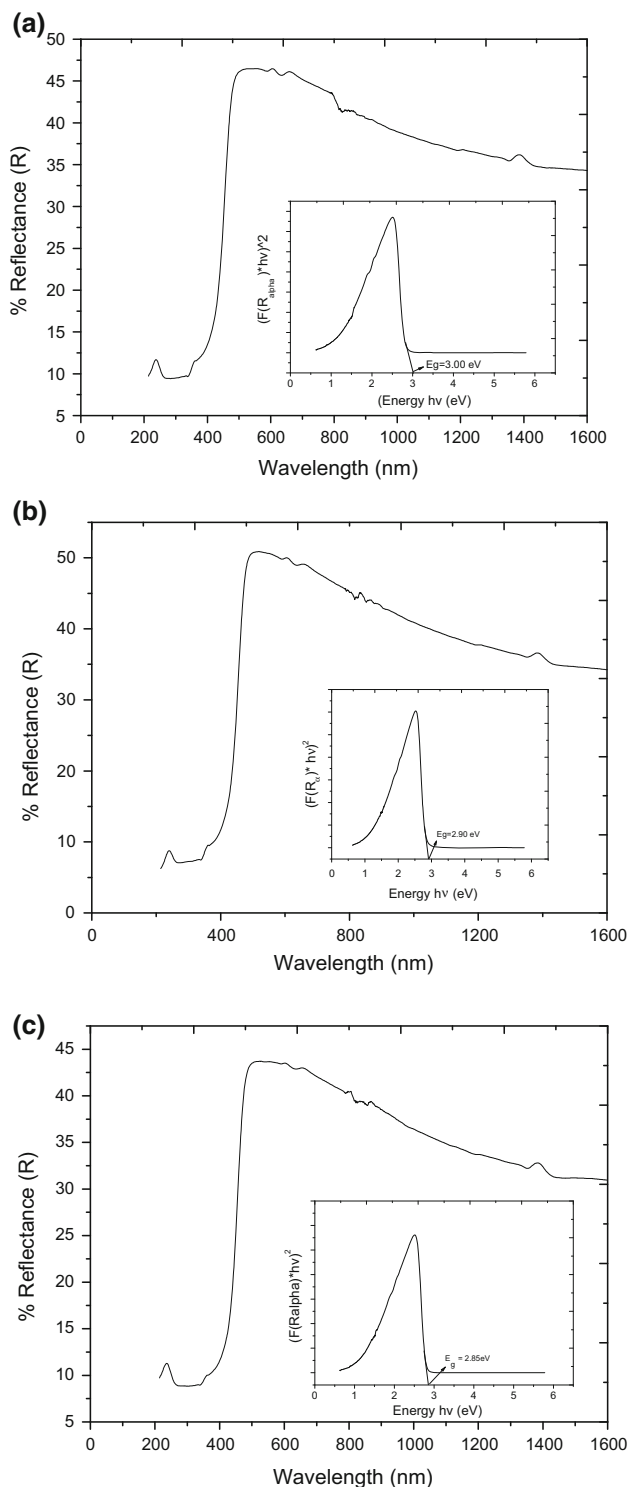$$\frac{K}{S} = \frac{(1-R_\infty)^2}{2R_\infty} = F(R_\infty)$$

F(R$_\alpha$) is the so called remission or K–M function, where

$$R_\infty = \frac{R_{sample}}{R_{standard}}$$

A graph is plotted between [F(Rα)hν]^2 versus hν and the intercept value gives the band gap energy E$_g$ [13] of the individual sample. The band gap energies were calculated for pure and 3, 10 wt% Ag doped WO$_3$ are tabulated. These values offer an excellent agreement with the reported value. Table 2 shows the bandgap energy for pure and Ag doped WO$_3$.

3.4 Scanning electron microscopy and EDAX analysis

Scanning electron microscope is a useful technique to determine the morphology and particle size of the samples. Figures 4a and 5a shows SEM image of pure and Ag doped WO$_3$ nanoparticles. It was clearly observed that both the samples show spherical morphology with average diameter of 1–1.5 µm and thickness of 80–100 nm. The particle size estimated from XRD results much smaller than the SEM

Table 1 Observed FTIR spectrum for pure and Ag doped WO$_3$

Reference value	Pure WO$_3$	3 wt% Ag doped	5 wt% Ag doped	Tentative assignment
1625.98	1620.45	1626.68	1623.98	W–OH
833.21	882.88	897.39	827.21	W–O–W bridging mode

Fig. 3 a UV–visible DRS spectra for pure WO_3. **b** UV–visible DRS spectra for 3 wt% Ag doped WO_3. **c** UV–visible DRS spectra for 10 wt% Ag doped WO_3

Table 2 Band gap energy for pure and Ag doped WO_3

Material	Bandgap energy (eV)
Pure WO_3	3.00
3 % Ag	2.94
5 % Ag	2.85

decreases when increasing the Ag content as shown in the Fig. 5a. The decrease of crystalline size was also confirmed by XRD results. The EDAX results confirm the obtained materials which are composed of W and O as shown in the Fig. 4b. Figure 5b shows the EDAX spectra for silver doped WO_3 that confirms the presence of silver in the synthesized material. The intensity peak of tungsten was decreased due to the addition of silver ions in the tungsten site and intensity peak of oxygen remains constant for both pure and Ag doped WO_3.
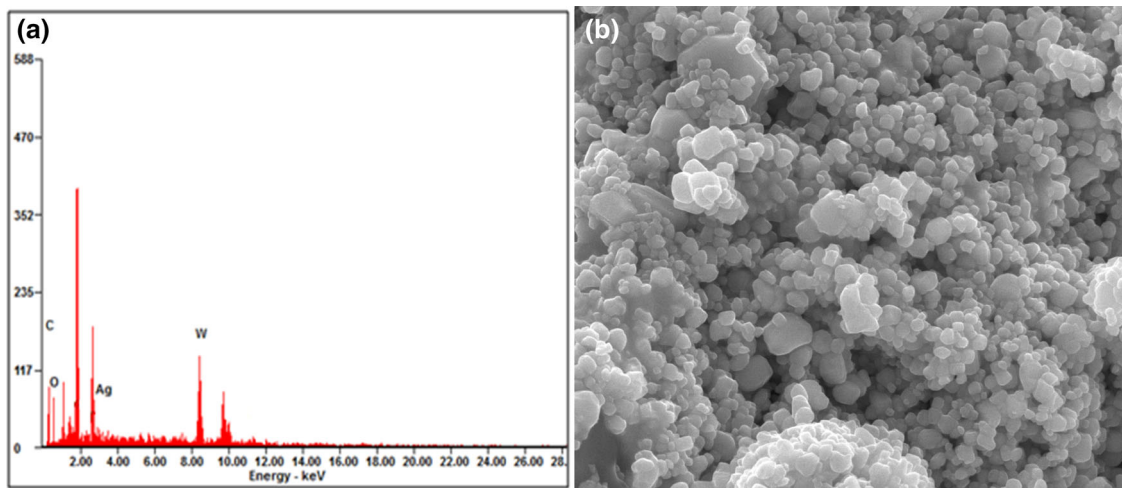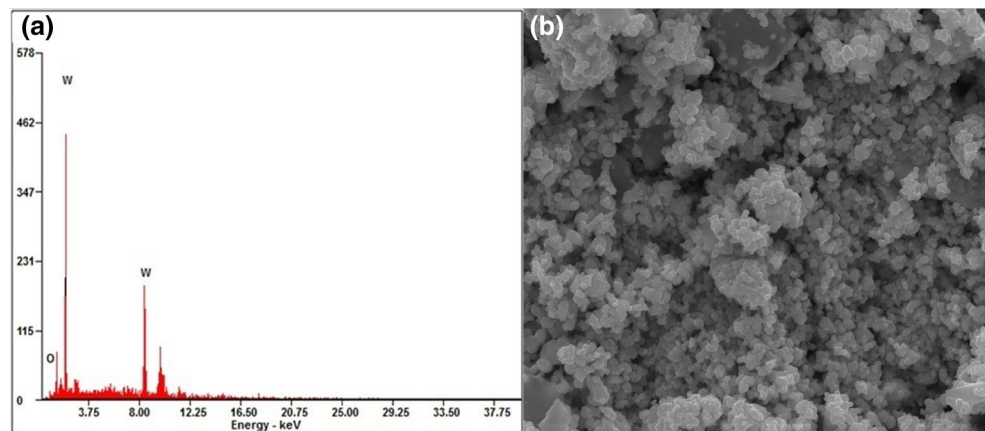
3.5 Transmission electron microscope

Figure 6a, b shows the TEM image of both pristine and Ag doped WO_3 nanoaprticles. It is clearly observed that both particle have spherical shaped morphology with an average diameter of about 30–40 nm for pure and Ag doped WO_3 nanoparticle which shows very good agreement with XRD result. The morphology of doped particles remain unchanged but the average diameter got decreased. Figure 6c, d show the SAED pattern and HRTEM image of Ag doped WO_3 nanoparticles. The SAED pattern confirms that the prepared material is well crystallized nanoparticles grown along the [002] direction [21]. The HRTEM images show that the interplanar distance of Ag doped WO_3 is 0.366 nm for the crystal plane [002] [22].

3.6 Photoluminescence studies

The PL spectroscopy is a useful study to measure the energy distribution of emitted photons after optical excitation and to understand the electron hole pair in the semiconducting oxide materials [23]. The oxygen vacancy and lattice distortion of pure and silver doped tungsten oxide samples were analyzed using photoluminescence spectra and it is shown in the Fig. 7. The spectra were recorded under the excitation wavelength of 325 nm at room temperature. Both pure and Ag doped tungsten oxide material show blue emission (485 nm) and green emission (558 nm). The blue emission is due to the defect level in the bandgap for its electron transition. The green emission peak (558 nm) is related to v_o^+ oxygen vacancies and these emission may be attributed to the different luminescent centers such as defect energy levels arising due to silver

results. This change in size could be due to the larger particles which are composed of many smaller particles. After doping of Ag dopant the plate like morphology

Fig. 4 SEM and EDX spectra of WO$_3$

Fig. 5 SEM and EDX spectra of Ag doped WO$_3$

interstitials and oxygen vacancies as well as dangling bonds into nanocrystals. Due to the silver doped into tungsten oxide, the intensity of peaks increases and shifted towards the higher energy. The increase in the peak intensity is due to the presence of Ag into WO$_3$ which cause lattice defects.

3.7 Photocatalytic activity set up

The photocatalytic activity set-up was fabricated by Vadivel et al. [24]. The photocatalytic experiment on the prepared samples for the photodegradation of dyes is performed at ambient temperature. The photocatalytic activities of pure and Ag doped WO$_3$ samples were evaluated by the degradation of methylene blue (MB), in visible light irradiation. For photocatalytic process, the dye solution was prepared by adding a particular concentration (for example 200 ml, $C_0 = 10$ mg l^{-1}) and a particular amount of synthesized material poured into dye solution. The 150 W high pressure mercury lamp was used as a light source. The samples/dye solution was

irradiated in the horizontal direction and the distance between the UV lamp and the glass/dye solution was kept within 25 cm. Then the solution was kept in the dark room and well stirred with magnetic stirrer for more than 60 min to attain the equilibrium condition throughout the solution. The concentration of the aqueous suspensions (MB) in each sample was analyzed by using UV–Vis spectrophotometer at a wavelength range of 300–600 nm. The photocatalytic efficiency was calculated from the expression $g = (1 - C/C_0)$, where C_0 is the initial concentration of dyes (MB) before illumination and C is the concentration of dyes after a certain irradiation time (15 min).

3.7.1 Photocatalytic activity measurements

The photocatalytic activities of pure and Ag doped WO$_3$ samples were evaluated based on their ability to degradation of methylene blue (MB) under visible irradiation. 2 g l^{-1} of pure WO$_3$ and Ag doped WO$_3$ nanoparticles were added to methylene blue (MB) to determine the

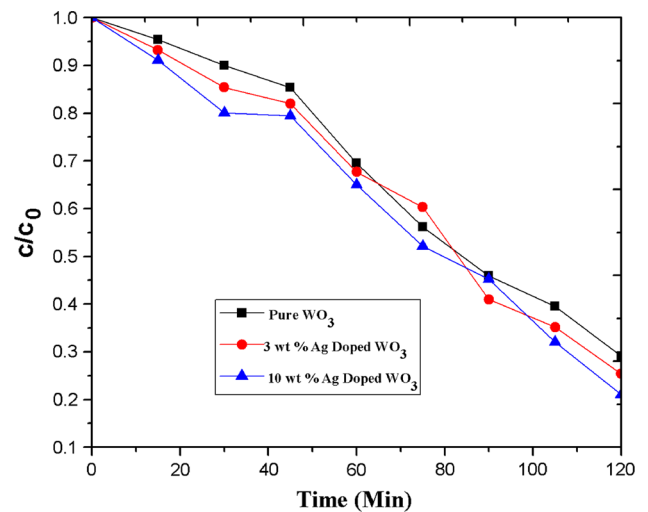**Fig. 6** TEM image of **a** pure WO$_3$ **b** 10 wt% Ag doped WO$_3$, **c** SAED pattern of Ag doped WO$_3$, **d** HRTEM image of Ag doped WO$_3$
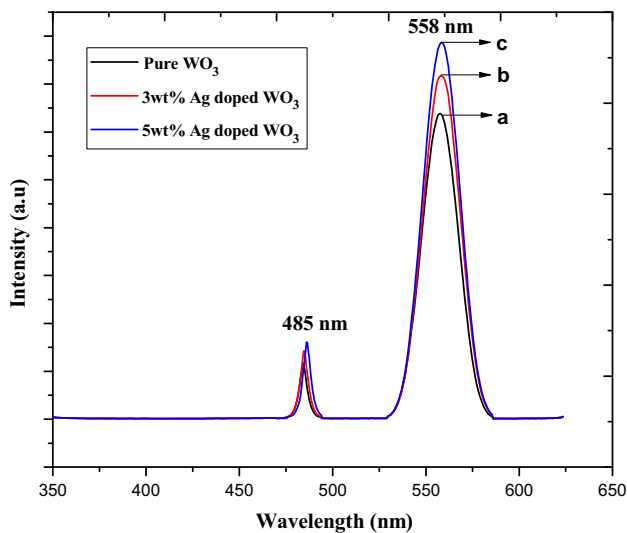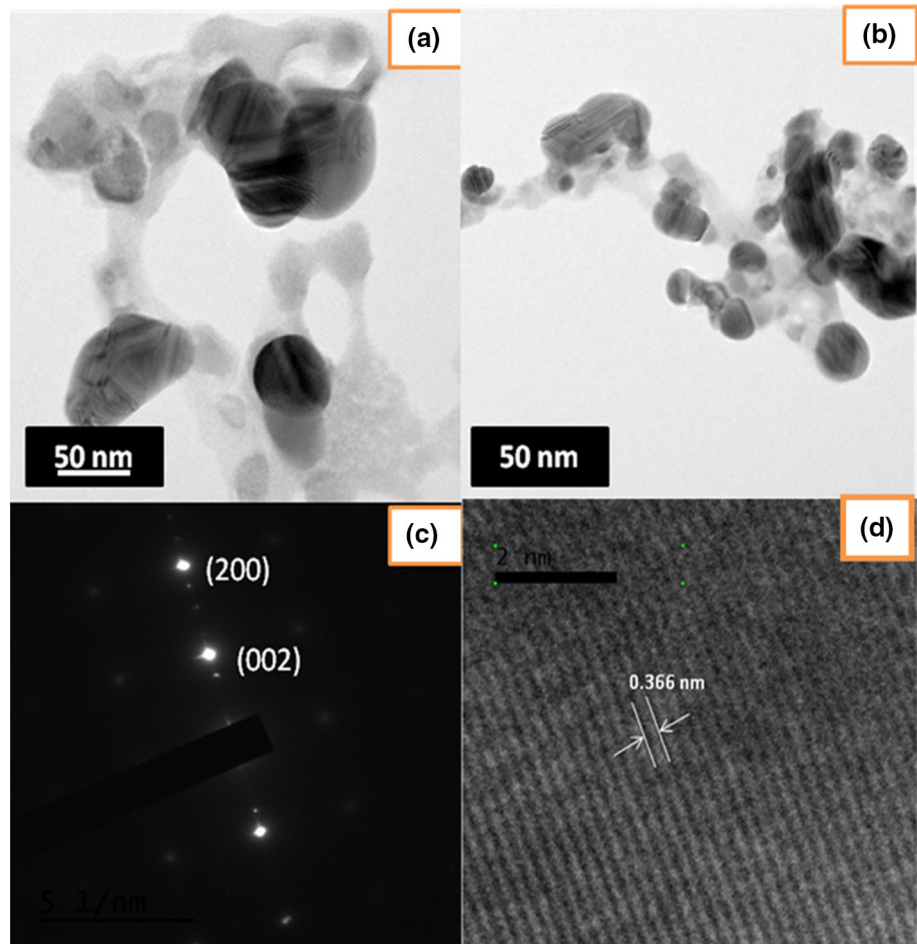
Fig. 7 Photoluminescence spectra for (*a*) pure WO$_3$, (*b*) 3 wt% Ag, (*c*) 10 wt% Ag

Fig. 8 Photocatalytic degradation of methylene blue (MB) using Mn–WO$_3$ catalyst under visible-light irradiation

efficiency in degradation. The results shows that the time of the illumination and the quantity of the photocatalyst used for the degradation of the MB dyes. In Fig. 8, the

graph is plotted between degradation percentage of MB dyes concentration in the aqueous sample after visible light irradiation in the presence of a typical pure and 2 g l^{-1} Ag
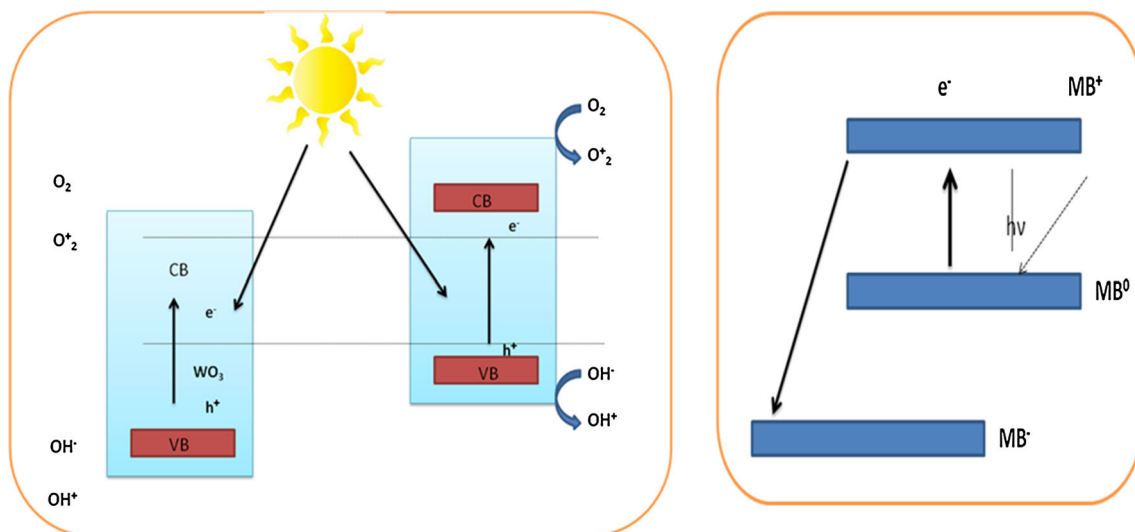
Fig. 9 Schematic diagram for representation for photocatalytic mechanism of MB in Mn doped WO$_3$ catalyst

doped WO$_3$ samples. The photocatalytic activity of Mn doped samples increased with the increase of Ag ion concentrations. Figures 8 represent the degradation of MB of WO$_3$ with different Ag concentrations (3 and 10 wt%). In my previous studies Mn doped WO$_3$ shows very good photocatalytic activity [12]. Comparing to the previous studies, the Ag doped WO$_3$ shows the better photocatalytic activity. Due to the lower bandgap energy compare to Mn doped WO$_3$ exhibit very good photocatalytic activity. With the reaction time at 150 min, the MB degradation efficiencies of pure and Ag (3 and 10 wt%) doped WO$_3$ samples are about 71,75 and 81 %, respectively.

Figure 9 shows the schematic representation of the mechanism of pure and Ag doped WO$_3$ in the degradation of methylene blue dye. The bandgap energy of pure tungsten oxide is lowered by the addition of manganese into the site of tungsten. Due to this factor the generation of electron and holes pair will increase and enhance the photocatalytic activity for Mn doped WO$_3$. The reaction between the Ag doped WO$_3$ with the photons as follows.

$$Ag-WO_3 + h\nu \rightarrow e\,CB^- + hVB^+$$
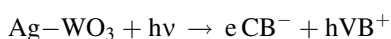
The system is irradiated with the photons (visible light) the electron in the valence band move to the conduction band of pure WO$_3$. In Mn doped material, the W^{6+} lattice position is replaced by Ag^{2+} ions, it will lower the conduction band of WO$_3$. As a result the Ag doped WO$_3$, electron can exhibit from the valence band of Ag energy level. Then the photogenerated electrons can easily transferred from the conduction band of Ag doping energy level to the surface of photocatalyst to capture adsorbed O$_2$ which improve the separation efficiency of charge carriers. This two factors give rise to the increase in photocatalytic efficiency for 10 wt% Ag doped WO$_3$ catalyst compared to

the pure WO$_3$. At the same time, more MB molecules are adsorbed on the surface of Ag–WO$_3$ catalyst, enhancing the photo excited electron to the conduction band and simultaneously increasing the electron transfer to the adsorbed O$_2$. Moreover the smaller bandgap energy due to Ag dopant can play another role in enhancing the visible light photocatalytic activity of WO$_3$ catalyst.

4 Conclusion

Finally, it has been substantiated that a simple and inexpensive microwave irradiation method is used to synthesise the pure and Ag doped WO$_3$. The crystalline size and structure were evaluated from XRD which has monoclinic structure and crystallite which ranges from 35 to 31 nm. TEM analysis shows both pristine and Ag doped WO3 nanoparticles are spherical shaped morphology with average particle size from 40 to 30 nm and it was compared and in very good agreement with the XRD result. The UV-DRS method was used to calculate the bandgap energies of the prepared material and it has an effective with the reported value. The bandgap energy value shows the emission of radiation in the visible region. Ag doping into the WO$_3$ reduces the bandgap which is evident by a red shift in the optical absorption edge and that was found by UV-DRS method. SEM confirms the plate like morphology change as the silver concentration increases in the WO$_3$. The energy dispersive spectrum confirms the presence of tungsten, oxygen and silver in the synthesized materials. UV-DRS analysis shows that the band gap energy decreases with the increase in the particle size. The PL studies show the red shifts in the optical absorption edge and the same was obtained for pure and Ag doped WO$_3$.

The photocatalytic activity of pure and Ag doped WO$_3$ catalysts were determined by degradation of MB under visible light irradiation. Ag doped catalysts show enhanced photocatalytic activity as compared with pristine WO$_3$. This Ag doped WO$_3$ catalyst may have potential applications in removal of pollutant as a highly efficient photocatalyst.

References

1. R. Abazari, A.R. Mahjoub, L.A. Saghatforoush, S. Sanati, Mater. Lett. **133**, 208–211 (2014)
2. S. Malato, P. Fernandez-Ibanez, M.I. Maldonado, J. Blanco, W. Gernjak, Recent overview and trends. Catal. Today **147**, 1–59 (2009)
3. M.A. Rauf, S.S. Ashraf, Fundamental principles and application of heterogeneous photocatalytic degradation of dyes in solution. J. Chem. Eng. **151**, 10–18 (2009)
4. A.R. Khataee, M.B. Kasiri, Photocatalytic degradation of organic dyes in the presence of nanostructured titanium dioxide: influence of the chemical structure of dyes. J. Mol. Catal. A Chem. **328**, 8–26 (2010)
5. S. Ahmed, M.G. Rasul, W.N. Martens, R. Brown, M.A. Hashib, Advances in heterogeneous photocatalytic degradation of phenols and dyes in wastewater: a review. Water Air Soil Pollut. **215**, 3–29 (2011)
6. H. Zhang, M. Feng, F. Liu, L. Liu, H. Chen, H. Gao, J. Li, Chem. Phys. Lett. **389**, 337–341 (2004)
7. L. Zhang, X. Tang, Z. Lu, Z. Wang, L. Li, Y. Xiao, Appl. Surf. Sci. **258**, 1719–1724 (2011)
8. M. Parthibavarman, K. Vallalperuman, S. Sathishkumar, M. Durairaj, K. Thavamani, A novel microwave synthesis of nanocrystalline SnO$_2$ and its structural optical and dielectric properties. J. Mater. Sci. Mater. Electron. **25**, 730–735 (2014)
9. X. Bai, H. Ji, P. Gao, Y. Zhang, X. Sun, Sens. Actuators, B **193**, 100–106 (2014)
10. S.B. Upadhyay, R.K. Mishra, P.P. Sahay, Sens. Actuators, B **193**, 19–27 (2014)
11. Z. Hua, M. Yuasa, T. Kida, N. Yamazoe, K. Shimanoe, Thin Solid Films **548**, 677–682 (2013)
12. S. Mohammed Harshulkhan, K. Janaki, Photocatalytic effect of manganese doped WO$_3$ and the effect of dopants on degradation of methylene blue. J. Mater. Sci. Mater. Electron. **26**, 8307–8314 (2015)
13. V. Hariharan, M. Parthibavarman, C. Sekar, Synthesis of tungsten oxide (W$_{18}$O$_{49}$) nanosheets utilizing EDTA salt by microwave irradiation method. J. Alloys Compd. **509**, 4788–4792 (2011)
14. T. Jesionowski, Characterisation of silicas precipitated from solution of sodium metasilicate and hydrochloric acid in emulsion medium. Powder Technol. **127**, 56–65 (2002)
15. D. Sanchez-Martinez et al., Characterization and photocatalytic properties of hexagonal and monoclinic WO$_3$ prepared via microwave-assisted hydrothermal synthesis. J. Mater. Res. Bull. **48**, 691–697 (2013)
16. M.H.S. Abhudhahir, J. Kandasamy, Synthesis and characterization of manganese doped tungsten oxide by microwave irradiation method. J. Mater. Sci. Semicond. Process. **40**, 695–700 (2015)
17. R. Yousefi, B. Kamaluddin, Fabrication and characterization of ZnO and ZnMgO nanostructures grown using a ZnO/ZnMgO compound as the source material. Appl. Surf. Sci. **256**, 329–334 (2009)
18. I. Hargittai, M. Hargittai, V.P. Spiridonov, E.V. Erokhin, An electron diffraction study on the vapors of tungsten trioxide. J. Mol. Strut. **8**, 31 (1971)
19. U. Opara Krasovec, A. Surca Vuk, B. Orel, Electrochim. Acta **46**, 1921 (2001)
20. A. Escobedo Morales, E. Sianchez Mora, U. Pal, Use of diffuse reflectance spectroscopy for optical characterization of un-supported nanostructures. Rev. Mex. Fis. **53**, 18–22 (2007)
21. Tomoharu Tokunaga, Tadashi Kawamoto, Kenta Tanaka, Yasuhiko Hayashi, Katsuhiro Sasaki, Kotaro Kuroda, Growth and structure analysis of tungsten oxide nanorods using environmental TEM. Nanoscale Res. Lett. **7**(1), 85 (2012)
22. W.H. Lai, J. Shieh, L.G. Teoh, M.H. Hon, Fabrication of one-dimensional mesoporous tungsten oxide. Nanotechnology **17**, 110–115 (2006)
23. Wu P, Q. Li, X. Zou, W. Cheng, D. Zhang, C. Zhao, L. Chi, T. Xiao, Correlation between photoluminescence and oxygen vacancies in In$_2$O$_3$, SnO$_2$ and ZnO metal oxide nanostructures. J. Phys. Conf. Ser. **188**, 012054 (2009)
24. S. Vadivel, G. Rajarajan, Effect of Mg doping on structural, optical and photocatalytic activity of SnO$_2$ nanostructure thin films. J. Mater. Sci. Mater. Electron. **26**, 3155–3162 (2015)